LATERAL CONFINEMENT EFFECT IN SHPB TEST OF THE SAP CONCRETE MATERIAL

Zhenqun SANG[1, 2], Zhiping DENG[1, 3*], Jianglin XI[4], Huibin YAO[2], Jiang WU[2]

The lateral inertia confinement effect and end face friction effect in Split Hopkinson Pressure Bar (SHPB) test of the Super Absorbent Polymers (SAP) concrete has been numerically studied based on the platform of ABAQUS. The numerical calculation of the lateral confinement effect in SHPB test for this SAP concrete revealed that lateral inertia confinement effect and end face friction effect both increase with the increase of the strain rate and decrease with the increase of porosity. At the same time, the reconstructed compressive strength just induced by lateral inertia confinement and end face friction effect can be obtained based on the numerical method, which lead to departure of the strain-rate effect of the material itself from the SHPB test.

Keywords: SAP Concrete Material; Lateral Confinement Effect; Strain-rate Effect; SHPB Test;

1. Introduction

The strain-rate effect of compressive strength in SHPB test on concrete materials can be attributed to the strain-rate effect of the material itself and lateral confinement effect, while the lateral confinement effect includes the lateral inertia confinement effect and end face friction effect [1-3]. Due to porosity and the inner cracks, the compressive and tensile strength of concrete materials vary with strain-rate, this effect coming from the material characteristics. The lateral confinement effect is more sensitive to test equipment and test condition, which can be considered as external causes for the strain-rate effect of compressive strength.

In SHPB test, it can be concluded that the compressive strength of Super Absorbent Polymers (SAP) [4-6] concrete [7-8] is sensitive to strain rate. The dynamic increase factor of compressive strength ($DIF\text{-}f_c$) can be defined as the ratio of compressive strength under high strain-rate f_c and compressive strength under quasi-static strain-rate f_{cs}, namely $DIF\text{-}f_c=f_c/f_{cs}$. The dynamic increase factor of compressive strength ($DIF\text{-}f_c$) increases with the increase of strain rate [9-10]. The quantitative research on the lateral confinement effect can deepen our

[1] Army Logistics University of PLA, Chongqing, 401311, China
[2] Communication Institute for NICOs, Army Engineering University of PLA, Chongqing, 400035, China
[3] Technology Brigade of Aerospace Engineering, Beijing, 100192, China
[4] Army Engineering University of PLA, Nanjing, 210007, China
[*] E-mail: dzpcorner@163.com

understanding of the strain-rate effect of the material itself and its mechanism [11-15], meanwhile it can provide a more accurate material parameter in the design of protection engineering. There is still a lack of relevant literature to discuss the lateral confinement effect in SHPB test on SAP concrete, which has the characteristics of porous materials.

In this paper, the lateral inertial confinement effect and end face friction effect in SHPB experiment of the SAP concrete have been studied based on the platform of ABAQUS.

2. Numerical Simulation of the Lateral Confinement Effect

2.1 Introduction to the Method

SAP concrete is a kind of porous material with spherical millimeter-size pores inside the mortar matrix. The average diameter of the saturated SAP is 5mm. In the process of curing, the spherical saturated SAP beads can slowly dehydrate and separate from the cement paste after shrinkage, and eventually leave closed millimeter-size pores evenly distributed in the concrete. SAP concrete have been used in the islands far from the mainland, to substitute the normal coarse aggregate with saturated SAP and reduce the cost with transportation of the normal aggregate.

Compressive strength of mortar matrix is related to hydrostatic pressure inside the materials just like the concrete materials; the compressive strength increases with the rise of hydrostatic pressure. This hydrostatic pressure correlation is the internal cause for the lateral confinement effect in SHPB test. In the numerical research, the "reconstitution" method is adopted, in which the reconstructed stress - strain curve of the SAP concrete specimens through SHPB test can be obtained based on the given quasi-static uniaxial compressive stress-strain curve of the mortar matrix. Many classical dynamic constitutive model of concrete can obtain the stress under dynamic loading σ_d based on the stress under quasi-static loading $\sigma_s(c)$ by introducing a enhancement factor $\dot{c}/\dot{c}_s$ $R(\dot{c})$ [13] , which is the ratio of the strength under dynamic loading σ_d and quasi-static loading $\sigma_s(c)$, into the constitutive equation, namely:

$$\sigma_d = \sigma_s(\mathrm{c})R(\dot{c}) \tag{1}$$

In "reconstitution" method, the material model is required to reflect the hydrostatic pressure correlation of the materials while not considering the strain-rate effect (namely the $R(\dot{c})$). So, this type of material model can simulate the influence of the lateral confinement on the stress - strain curve under dynamic loading. The variation between input stress-strain curve and reconstructed curve can reveal the degree of deviation from basic assumptions for SHPB experimental. The utilization of the material model not containing strain-rate

effect of the material itself can attribute the strength enhancement effect in SHPB test to other interference factors, such as friction, axial and lateral inertia effect and so on.

2.2 Material Model of the Mortar Matrix

The numerical research conducted in this paper is mainly based on the experimental data of SHPB test of the SAP concrete with different porosities, which are 10%, 20%, 30% and 40% respectively, and under quasi-static loading or dynamic loading with three strain rate levels of 70/s, 100/s and 140/s.

Table 1

Mechanical properties of SAP concrete subjected to quasi-static and high strain-rate loading

Theoretical porosity [%]	Real porosity [%]	Quasi-static strength [MPa]	Average strain rate [s^{-1}]	Compressive strength [MPa]	DIF-f_c
			79.7	95.4	1.78
10	9.5	53.6	107.6	102.4	1.91
			140.2	108.8	2.03
			68.2	68.2	1.80
20	19.3	37.9	100.0	74.7	1.97
			126.9	80.3	2.12
			70.5	40.1	1.92
30	27.8	20.9	104.7	45.1	2.16
			142.7	50.8	2.43
			72.1	30.7	1.97
40	38.7	15.6	101.5	36.0	2.31
			141.5	40.2	2.58

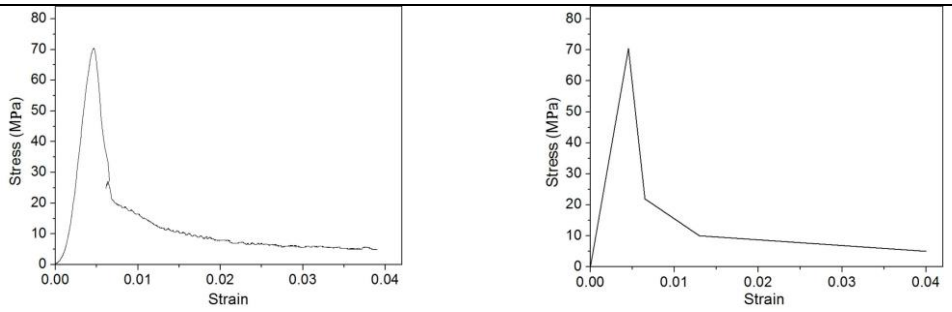

(a) Experimental stress-strain curve (b) Simplified stress-strain curve

Fig. 1 Quasi-static uniaxial stress-strain curve of the mortar matrix

The corresponding mechanical performance data of the SAP concrete is shown in Table 1. The uniaxial compressive stress-strain curve under quasi-static loading of the mortar matrix is shown in Fig. 1 (a), and this typical stress-strain curve can be simplified as shown in Fig. 1 (b). In the generic numerical simulation

software ABAQUS, the expanded Drucker-Prager model can describe the characteristics of the stress-strain relationship shown in Fig. 1, and can also reflect the hydrostatic pressure correlation of compressive strength for the material while not considering the strain-rate effect.

2.3 Expanded Drucker-Prager Model

The expanded Drucker-Prager model used in ABAQUS is obtained from the classic Drucker-Prager elastoplastic model [16], which can reflect the stress flow phenomenon of concrete due to internal friction associated with confining pressure. Thus, the expanded Drucker - Prager model can better simulate the strength increase with rise of confining pressure in concrete materials, and it can be used to calculate the deformation development during the process of strain hardening and strain softening in the framework of large deformation dynamics. The expanded Drucker - Prager model and dynamic finite element algorithm used in this paper are based on general computing platform of ABAQUS to eliminate the differences in numerical calculation by different organizations, so that the follow-up or other people's work can be compared.

3. Establishment of the Numerical Model

3.1 Simplified SHPB Device

The measured incident wave in SHPB experiment is set as the input of numerical model to reduce model complexity and the amount of calculation, which will also reduce the difference between numerical simulation and experiment. In the numerical model, the simplification of the SHPB experimental device is as following: the conical cross-section of incident bar is simplified to uniform square section; the length of the incident bar is reduced to 800mm from the original 3200mm; the length of the transmitted bar is reduced to 800mm from the original 1600mm. The contraction in length of the incident bar and transmitted bar can reduce the amount of computation and the time of computation in condition of guaranteeing the accuracy and at least a full waveform transmitting in the bars. The simplified test device is shown in Fig. 2, in which the location of the strain gauge has considered the velocity and transmission time of the stress wave in the bar. Thus, the recorded stress wave will not be superimposed by the reflected wave on the interferences to obtain the full waveform. The “two wave method” has been used to reconstruct the stress - strain curve of the specimen.

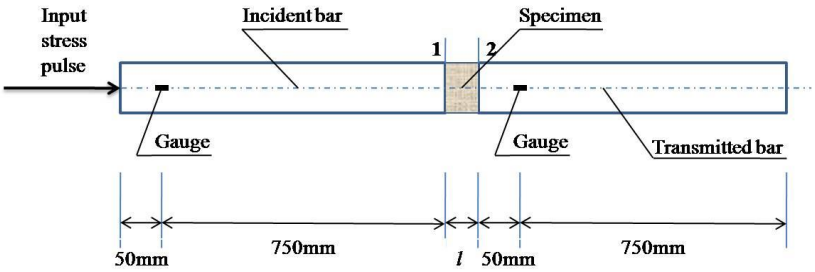

Fig. 2 Schematic diagram of the SHPB set-up for numerical simulation

3.2 Parameters of the Material Model

The density of the pressure bar is known, and the linear elastic model is used to describe its mechanical property; the relevant physical parameters are shown in Table 2.

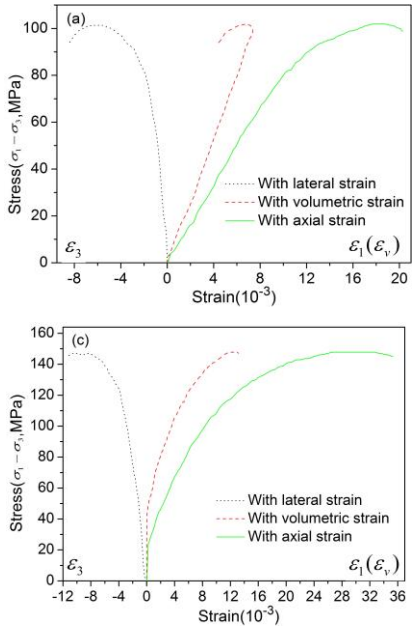

Fig. 3 Stress-strain curves in triaxial tests ((a),(b),(c) is with the confining pressure of 14MPa, 28MPa and 42MPa respectively)

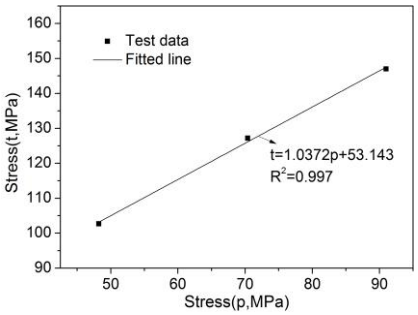

Fig. 4 Fitting curve of the average strength data in triaxial tests

The mechanical parameters of the mortar matrix under uniaxial compression can be obtained from Figure 1, while the parameters such as the friction angle β and the dilatancy angle Ψ of the expanded Drucker - Prager model should be determined by a triaxial test. The compressive mechanical behavior under confining pressure of 14MPa, 28MPa and 42MPa has been tested using a rock triaxial test system with cylindrical specimens having a diameter of 50mm

and height of 100mm. During the triaxial test, the specimens were under uniform confining (σ_2=σ_3) firstly and then the axial pressure stress σ_1 was loaded on the specimens. The stress difference $\sigma_1 - \sigma_3$, axial strain ε_1, lateral strain ε_3 and volume strain ε_v=ε_1+2ε_3 have been recorded during the test, in order to obtain the relation between the additional stress σ_1 and the volume strain ε_v. A partial test result is shown in Fig.3. A fit of the average compressive strength under different confining pressure in the p - t plane (p is equivalent hydrodynamic pressure, t is deviatoric stress) using linear fit is shown in Fig.4, from which the friction angle for 46 ° of expanded Drucker-Prager model can be deduced. Park [17] has found that the influence of dilatancy angle on the simulation of SHPB experiment can almost be ignored in their numerical research on the impact property of mortar plate using the expanded Drucker - Prager model. Thus, the value of dilatancy angle Ψ can be equal to the friction angle β, which means that the deviatoric plane parameter is K=1, indicating an associated flow rule of the model [18]. In Table 2, the density, elastic modulus, Poisson ratio and compressive strength of the mortar matrix are listed as the average value obtained for each specimen in triaxial test.

Table 2

Material properties involved in the numerical model

Material	Density [kg/m^3]	Elastic modulus [GPa]	Poisson ratio	Compressive strength [MPa]	Friction angle β	Dilatancy angle Ψ	K
Pressure bar	7850	210	0.3	400	—	—	—
Mortar matrix	2172	24.2	0.21	70.5	46°	46°	1

3.3 The input Stress Pulse

Based on the SHPB test of SAP concrete with different porosities under three different strain rate levels [9], the recorded incident stress waves in the tests have been loaded as input stress pulse on the incident bar of the SHPB set-up shown in Fig. 2.

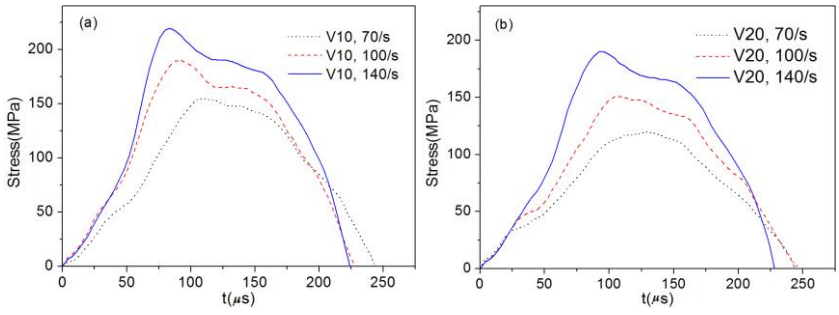

(a) Specimen with porosity 10% (b) Specimen with porosity 20%

Fig. 5 Input stress wave pulse on the input end of the incident bar

The typical incident stress waves for specimens with 10% and 20%

porosity under different strain rates in the SHPB test are shown in Fig. 5.

3.4 Mesh Generation

To improve the mesh quality for dynamic calculation, the cross - section shape of the pressure bar and specimen should be simplified: 1) for the pressure bar, the circular cross - section was simplified to square cross - section with original cross - section area, length and volume; 2) the cylinder specimen was simplified to rectangular shape with the same thickness and volume. The compressive strength of circular cross-section and square cross-section specimens of mortar matrix have been tested under strain rate level of 70/s. The result is shown in Fig. 6, in which the compressive strength and stress - strain curve are close to each other. Thus, it is acceptable to use square cross - section specimen in numerical calculation.

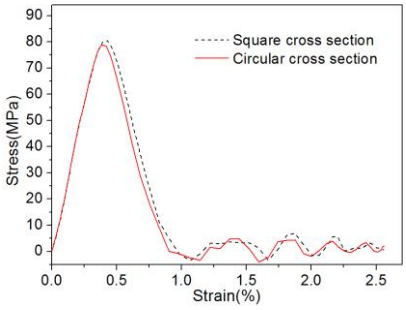

Fig. 6 Stress-strain curve of specimens with circular and square cross section in SHPB test.

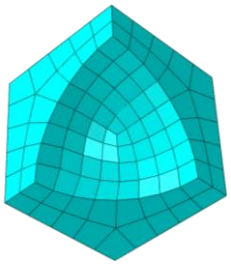

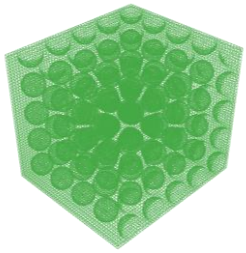

(a)One-eighth of a cell (b) The meshed specimen

Fig. 7 Mesh of one-eighth of the unit cell and specimen with porosity 20%

Table 3

Parameter of the finite element model for specimen

Hole diameter [mm]	Theoretical porosity[%]	Real porosity [%]	Simulation porosity [%]	Size of the cell [mm]	Number of holes	Number of elements
5	10	9.5	9.5	8.7656×8.7656×8.7656	196	84672
	20	19.3	19.7	7.000×6.8930×6.8930	405	88290
	30	27.8	29.2	5.9033×6.1667×6.1667	600	76800
	40	38.7	38.5	5.700×5.4624×5.4624	792	101376

A trial calculation indicated that the mesh quality around the pores was the main factor that influences the precision of calculation. To avoid hourglass effect during calculation, the mesh quality must be guaranteed strictly. The structured mesh technology and C3D8R (eight nodes three-dimensional stress reduced integral unit) have been adopted to mesh the incident bar, transmitted bar and specimens. Thus, the random holes originally contained in the mortar must be arrayed in the numerical model based on the structured mesh, and the meshed specimen possesses symmetry. The mesh of one-eighth of a cell and the meshed

specimen with porosity 20% are shown in Fig.7. Based on symmetry, this paper only establishes a one-fourth model, which requires symmetrical boundary conditions. The mesh parameters for specimen with different porosities are shown in Table 3.

4. Lateral Confinement Effect

4.1 Lateral Inertia Confinement Effect

Without regard to the friction of the interface of specimen and bars (namely the friction coefficient of the interface has been set to zero in the numerical model), the reconstructed stress-strain curve, and average hydrostatic curve can be obtained through the numerical calculation. Fig.8 shows the results for specimen with 20% porosity under strain-rate level 100/s. The increment $\Delta f_{c,lat}$, which is the difference between the reconstructed compressive strength and quasi-static compressive strength, varies with porosity and strain rate levels as shown in Fig.9 and Fig.10. The peak values p_c of the average hydrostatic pressure curve for specimens with different porosities and strain rate levels are displayed in Fig.11 and Fig. 12.

Fig.9 and Fig.10 show that, under the same strain rate levels, the reconstructed compressive strength increment $\Delta f_{c,lat}$ decreases with the rise of porosity, which indicates that the growth of compressive strength is more close to the response of the material itself for high porosity specimens in SHPB test. For the same porosity, the reconstructed compressive strength increment $\Delta f_{c,lat}$ of the SAP concrete specimen increases with rise of strain rate. The increment $\Delta f_{c,lat}$ with rise of strain rate of specimen with lower porosity is larger than that of specimen with relatively high porosity, which indicates that the reconstructed compressive strength increment $\Delta f_{c,lat}$ is more sensitive to strain rate for specimen with low porosity.

Fig.11 and Fig.12 shows that, under the same strain rate, the peak value of the average hydrostatic pressure curve decreases with increase of porosity. For a given porosity, the peak value of average hydrostatic pressure increases with the increase of strain rate. The variation trend of peak value of the average hydrostatic pressure curve with porosity and strain rate is consistent with reconstructed compressive strength increment. In Fig.11, the four dotted lines represent 1/3 of the quasi-static compressive strength of SAP concrete specimens. It can be concluded form Fig.11 that, for each of the three high strain rate levels and four porosities, the peak value of the average hydrostatic pressure surpasses 1/3 of the quasi-static compressive strength and is even bigger than 1/2 of the quasi-static compressive strength. The peak value of average hydrostatic pressure is higher than 1/3 quasi-static uniaxial compressive strength $f_{c,qua}$, which means that: 1) the other two principal stress σ_2, and σ_3 are not equal to zero; 2) the specimen inside is

not in uniaxial stress state; 3) the inertia effect is significant. The strain-rate effect caused by crack and friction between specimen and bars has not been accounted in the simulation. According to the expanded Drucker-Prager model, the compressive strength of concrete increases with increase of hydrostatic pressure. The inertia effect under high strain rate limits the lateral extension of the specimen and forms a lateral confinement. Thus, the strain-rate effect of compressive strength in SHPB test for SAP concrete is not all the response of the material itself, while it contains increase of the compressive strength caused by lateral inertial confinement effect under impact loads, which is difficult to rule out by experiment means.

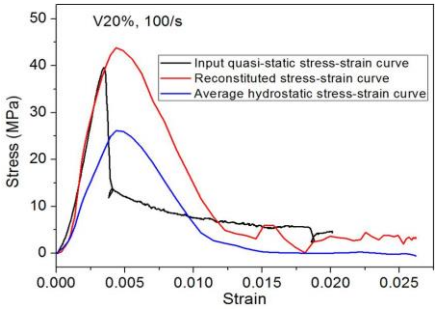

Fig. 8 Reconstituted stress-strain curve of the specimen

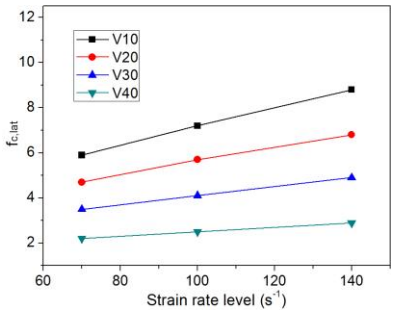

Fig. 9 Variation of $\Delta f_{c,lat}$ with strain rate

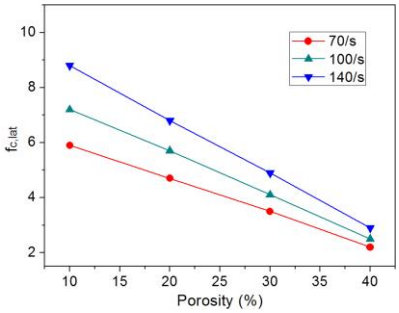

Fig. 10 Variation of $\Delta f_{c,lat}$ with porosity

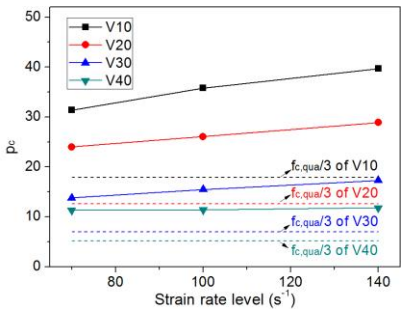

Fig. 11 Variation of p_c with strain rate

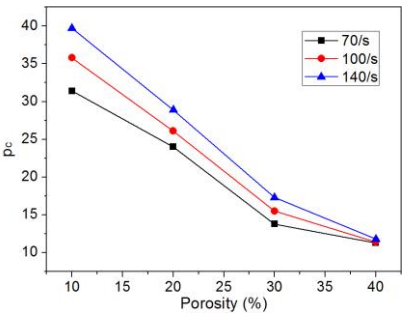

Fig. 12 Variation of p_c with porosity

4.2 End Face Friction Effect

Berthold and Karnes [19] have studied the influence of friction between the interfaces of the specimen and pressure bars on the result of SHPB test using numerical simulation method and shown that important stress and strain non-uniformity exists when the interfaces are not lubricated properly. Moreover, the research about friction of the interface in SHPB test was based on metal specimens, in which friction is usually smaller than that of concrete materials. As for concrete, in the SHPB test, smoothness of the end surface is unable to reach the standard of metal specimen. The friction effect cannot be ignored even with lubrication measures to reduce the friction coefficient.

In order to study the influence of end face friction on SHPB experimental results for SAP concrete with different porosities under different strain rates, the friction coefficient of the contact surface between SAP concrete specimen and pressure bar and is set to 0.05, 0.1, 0.2, 0.1 and 0.2 respectively, using contact face definition in ABAQUS. The reconstructed stress - strain curve can be calculated based on the numerical model built for research of the lateral confinement effect. Then, the reconstructed compressive strength $f_{c,lat\text{-}\mu}$, which contains the lateral inertia confinement effect and end face friction effect, can be obtained based on the reconstructed stress - strain curve. The increment of reconstructed compressive strength $\triangle f_{c,lat\text{-}\mu}$, which is the difference between $f_{c,lat\text{-}\mu}$ and quasi-static compressive strength and contains the end face friction effect only, can be obtained based on the reconstructed strength $f_{c,lat\text{-}\mu}$ and $f_{c,lat}$, namely:

$$\Delta f_{c,lat-\mu} = f_{c,lat-\mu} - f_{c,lat} \tag{2}$$

For a given strain rate level, the increment of reconstructed compressive strength $\triangle f_{c,lat\text{-}\mu}$ varies with end face friction, and the variation is shown in Fig.13 for specimens with different porosities (just porosity 10% and 20% is shown).

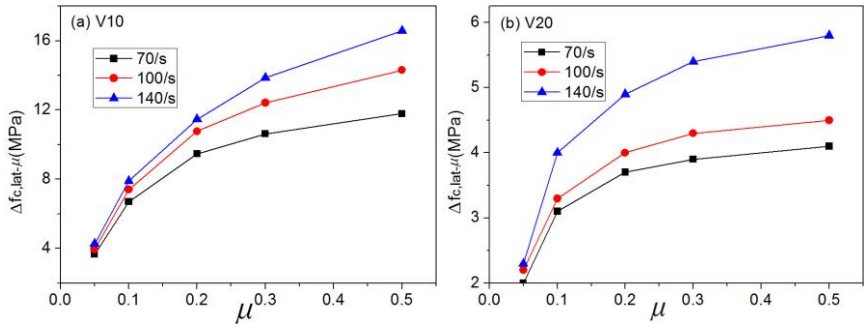

Fig. 13 Variation of $\Delta f_{c,lat\text{-}\mu}$ with friction coefficient

Fig.13 shows that the increments of reconstructed compressive strength $\triangle f_{c,lat\text{-}\mu}$ are all greater than zero, which indicates that the influence of end face friction on the compressive strength should not be neglected. The increments of

reconstructed compressive strength $\triangle f_{c,lat\text{-}\mu}$ caused by end face friction increases with rise of end face friction. The increase speed of $\triangle f_{c,lat\text{-}\mu}$ with friction coefficient below 0.2 is relatively high, while the speed slows down gradually when the friction coefficient surpasses 0.2. For a given friction coefficient and porosity, $\triangle f_{c,lat\text{-}\mu}$ increases with strain rate indicating a significant influence on the compressive strength of end face friction under high strain rates. For low porosity specimens, when the friction coefficient is greater than 0.2, the impact of friction on compressive strength is significant, so it is necessary to reduce the friction coefficient in SHPB experiment.

4.3 Strain Rate Effect of the Material Itself

The increase of compressive strength in the SHPB test under high strain rate can be attributed to the strain-rate effect of the materials itself, lateral inertia confinement effect and end face friction effect. In the SHPB experiment, the dynamic strength increases factor $DIF\text{-}f_c$ of compressive strength (Dynamic Increase Factor, it is the ratio of compressive or tensile strength under dynamic loading and quasi-static loading) obtained from the test can be expressed as:

$$DIF\text{-}f_c = f_{cd} / f_{cs} = (\Delta f_{cd} + f_{cs}) / f_{cs} \tag{3}$$

in which, $\triangle f_{cd}$ is the increment of dynamic compressive strength caused by the strain rate effect coming from lateral inertia confinement effect, end face friction effect and strain rate effect of the materials itself, and f_{cs} is the compressive strength under quasi-static loading. The compressive strength f_{cs} under quasi-static loading also increases with rise of the loading rate, which usually contributes to the cyclo-hoop effect. Assuming that the dynamic compressive strength increment $\triangle f_{cd,r}$ caused by the material itself is not associated with $\triangle f_{c,lat\text{-}\mu}$, $\triangle f_{cd}$ can be represented as:

$$\Delta f_{cd} = \Delta f_{cd,r} + \Delta f_{cd,lat-\mu} \tag{4}$$

Bringing equation (4) into (3):

$$DIF\text{-}f_c = (\Delta f_{cd,r} + \Delta f_{cd,lat-\mu} + f_{cs}) / f_{cs} \tag{5}$$

If the strain-rate effect of the material itself is not taken into account, the dynamic strength growth factor of the compressive strength $DIF\text{-}\triangle f_{c,lat\text{-}\mu}$ is caused by lateral inertial confinement effect and end face friction effect. Thus, the increase of the factor $DIF\text{-}\triangle f_{c,r}$ caused by the strain rate effect of the material itself is:

$$DIF\text{-}f_{c,r} = DIF\text{-}f_c - DIF\text{-}f_{cd,lat-\mu} \tag{6}$$

Paper [13] shows that the friction coefficient between the concrete specimen and steel pressure bar in SHPB test can be reduced to about 0.1 by

applying lubrication properly. Thus, the increment of the reconstructed compressive strength $\triangle f_{c,lat\text{-}\mu}$ can be obtained from Figure 8 with friction coefficient 0.1 to deduce the value of $DIF\text{-}\triangle f_{c,lat\text{-}\mu}$ and $DIF\text{-}\triangle f_{c,r}$, which are shown in Fig.14, respectively.

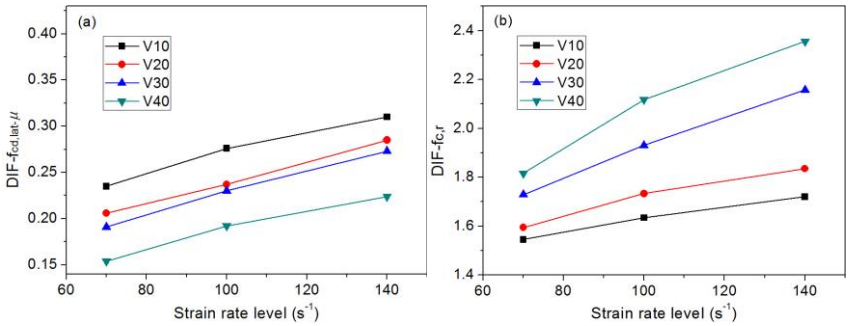

Fig. 14 DIF-$f_{cd,lat\text{-}\mu}$ and DIF-$f_{c,r}$ of specimens with different porosity under three strain rate levels

As shown in Fig.14, $DIF\text{-}\triangle f_{c,r}$ increases with increase of porosity and indicates an obvious strain rate effect. The $DIF\text{-}\triangle f_{c,lat\text{-}\mu}$ increases with porosity, which reflects that the influence of lateral inertial confinement effect and end face friction effect is larger for specimen with low porosities. At the same level of the strain rate, $DIF\text{-}\triangle f_{c,r}$ increases with increase of porosity, which show that the specimen with high porosity has a more significant strain rate effect of material itself, and it is consistent with SHPB experiment results.

Table 4

Parameter of the fittig equation

Theoretical porosity (%)	Parameter a	Parameter b
10	0.1499	0.1548
20	0.0746	0.2034
30	0.0141	0.3190
40	0.0063	0.3761

The variation of dynamic strength increase factor of the material itself with strain rate for SAP concrete specimens with different porosities can be fitted as equation (7), and the result is shown in Fig.15, which shows a linear relation between $DIF\text{-}f_{c,r}$ and the relative strain rate $\dot{c}/\dot{c}_s$ ($\dot{c}$ is high strain rate, $\dot{c}_s$ is the quasi-static strain rate) in double logarithmic coordinates. The fitting equation is:

$$DIF\text{-}f_{c,r} = a\left(\frac{\dot{c}}{\dot{c}_s}\right)^b \tag{7}$$

where the coefficients a and b are listed in Table 4.

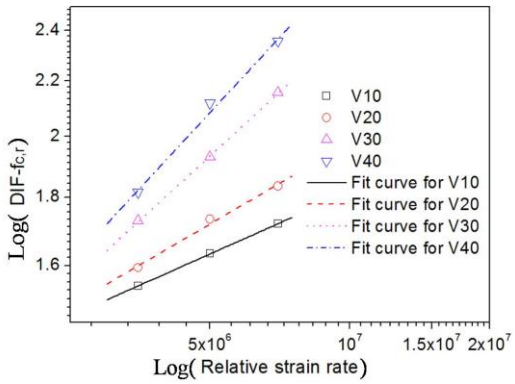

Fig. 15 Variation of *DIF*-$f_{c,r}$ with relative strain rate the corresponding fitting curve.

5. Conclusion

(1) The influence of lateral inertia confinement effect on the dynamic compressive strength cannot be ignored in SHPB experiments.

(2) The increment of compressive strength $\triangle f_{c,lat}$ caused by lateral inertia confinement effect decreases with increase of porosity indicating that the strain rate effect is more close to the strain rate effect caused by material itself for SAP concrete with high porosity than that with relatively low porosity.

(3) The strain rate effect of compressive strength in SHPB test for SAP concrete is not only the response of the material itself, while it contains increase of the compressive strength caused by lateral inertial confinement effect.

(4) The increment of compressive strength $\triangle f_{c,lat\text{-}\mu}$ caused by end face friction increases with the rise of strain rate, and decreases with increase of porosity under a given strain rate level and friction coefficient.

(5) Lateral inertial confinement effect and end face friction effect have more influence on the compressive strength of the specimen with relatively low porosity. The strain rate effect caused by the concrete material itself is more significant for SAP concrete with high porosity.

Acknowledgements

We are indebted to the Chinese Natural Science Foundation Project of CQ CSTC（cstc2014jcyjA50026）and the Graduate Student Innovation Fund of Chongqing (CYB16127) for support of this research.

R E F E R E N C E S

[1]. *W.F. Brace, A.H. Jones.* Comparison of uniaxial deformation in shock and static loading of three rocks. Journal of Geophysical Research Atmospheres, 1971, 76(20): 4913-4921.

[2]. *C. Young, C.N. Powell.* Lateral inertia effects on rock failure in split Hopkinson-bar experiments. U.S. Symposium on Rock Mechanics, 1979, 4: 231-241.

[3]. *P.H. Bischoff, S.H. Perry.* Compression behavior of concrete at high strain-rates. Materials and Structures. 1991, 24: 425-450

[4]. X.M. Kong, Z.L. Zhang, Z.C. Lu. Effect of pre-soaked superabsorbent polymer on shrinkage of high-strength concrete. Materials and Structure, 2015, 48 (9): 2741- 2758.

[5]. G.R.D. Sensale, A.F. Goncalves. Effect of fine LWA and SAP as internal water curing agents . International Journal of Concrete and Structure Materials, 2014, 8 (3): 229-238.

[6]. S. Laustsen, M.T. Hasholt, O.M. Jensen. Void structure of concrete with superabsorbent polymers and its relation to frost resistance of concrete. Materials and Structure, 2013, 48 (1-2): 357- 368.

[7]. *J. Yang, F.Z. Wang, Y.P. Liu.* CoMParison of ordinary pores with internal cured pores produced by superabsorbent polymers. Advanced Materials Research, 2015, 1129: 315-322.

[8]. *F.Z. Wang, J. Yang, S.G. Hu, X.P. Li, H.* Cheng. Influence of superabsorbent polymers on the surrounding cement paste. Cement and Concrete Research, 2016, 81: 112-121.

[9]. *Z.P. Deng, H. Cheng, Z.G. Wang, G.H. Zhu, H.S. Zhong.* Compressive behavior of the cellular concrete utilizing millimeter-size saturated SAP under high strain-rate loading. Construction and building materials, 2016, 119: 96-106.

[10]. *Z.P. Deng, H. Cheng, G.H. Zhu.* Dynamic behavior and constitutive model of super absorbent polymer concrete under impact loading. International journal of earth sciences and engineering, 2015, 8(6): 2974-2980.

[11]. *J.F. Georgin, J.M. Reynouard.* Modeling of structures subjected to impact: concrete behaviour under high strain rate. Cement and Concrete Composites, 2003, 25(1): 131-143.

[12]. *F.V. Donze, S.A. Magnier, L. Daudeville, C. Mariotti, L. Davenne.* Numerical study of compressive behavior of concrete at high strain-rates. Journal of Engineering Mechanics, 1999, 125(10): 1154-1163.

[13]. *Q.M. Li, H. Meng.* About the dynamic strength enhancement of concrete-like materials in a split Hopkinson pressure bar test [J]. Solids and structures, 2003, 40: 343-360.

[14]. *S.S. Yu, Y.B. Lu, Y. Cai.* A numerical method to determine real strain-rate effect for rock-like materials. Chinese journal of rock mechanics and engineering, 2013, 32(Supp.2): 3283-3290.

[15]. *Q. Fang, J. Hong, J.H. Zhang, L. Cheng, Z. Ruan.* Issues of SHPB test on concrete-like material. Engineering Mechanics, 2014, 31(5): 1-13

[16]. *D.C. Drucker, W. Prager.* Soil mechanics and plastic analysis or limit design [J]. Quarterly of Applied Mathematics, 1952, 10: 157-165.

[17] S.W. Park, Q. Xia, M. Zhou. Dynamic behavior of concrete at high strain rates and pressures: II. numerical simulation. International Journal Impact Engineering, 2001, 25(9): 887-910.

[18] D.C. Drucker, W. Prager. Soil mechanics and plastic analysis or limit design. Quarterly of Applied Mathematics, 1952, 10: 157-165.

[19]. *L.D. Bertholf, C.H. Karnes.* Two-dimensional analysis of the split Hopkinson pressure bar system. Journal of Mechanics and Physics of Solids, 1975, 23: 1-19.